Quantum simulations and *ab initio* electronic structure studies of $(H_2O)_2^-$

R. N. Barnett and Uzi Landman
School of Physics, Georgia Institute of Technology, Atlanta, Georgia 30332

S. Dhar and N. R. Kestner
Department of Chemistry, Louisiana State University, Baton Rouge, Louisiana 70803

Joshua Jortner and Abraham Nitzan
School of Chemistry, Sackler Faculty of Exact Science, Tel Aviv University, Tel Aviv 69978, Israel

(Received 19 June 1989; accepted 28 August 1989)

The energetics of the negatively charged water dimer $(H_2O)_2^-$, is studied using quantum-simulation techniques and *ab initio* electronic structure calculations. Using the RWK2-M potentials for water and a pseudopotential for the interaction of an electron with a water molecule in the ground state, consisting of Coulomb, adiabatic polarization, exclusion, and exchange contributions, it was found via the quantum path-integral molecular dynamics and the coupled quantum-classical time-dependent self-consistent field methods that while the minimum energy of $(H_2O)_2^-$ corresponds to a nuclear configuration similar to that found for the neutral $(H_2O)_2$ cluster, other nuclear configurations are also exhibited at finite temperature, characterized by a higher total molecular cluster dipole moment and a larger magnitude of the excess electron binding energy. Quantitative agreement is found between the results obtained by the quantum simulations, employing the excess electron–molecule pseudopotential, and those derived, for selected nuclear configurations, via *ab initio* calculations, employing the Gaussian 86 code with the basis set for the water molecules supplemented by a large diffuse set located at the midpoint of the two oxygens and in addition by a diffuse set for the excess electron.

I. INTRODUCTION

Recent experimental[1–10] and theoretical[11–36] investigations of nonreactive electron attachment to small clusters open new avenues for studies of electron localization and solvation in atomic and molecular systems and of the general issues of size effects on chemical and physical phenomena. Of particular interest in this context are questions pertaining to the modes[17–35] and dynamical mechanisms[32] of electron localization in finite aggregates and their spectroscopic consequences[29–33] and of the minimal cluster sizes which sustain bound states of an excess electron.[19,20,27,28,34]

Experimentally, gas-phase clusters containing an excess electron [polar molecular clusters of water[1,2,4–6] $(H_2O)_n^-$ and ammonia[3] $(NH_3)_m^-$, and ionic clusters[8–10] (Na_nCl_{n-1})] have been prepared and their mass dependent abundances have been investigated using time-of-flight mass spectroscopy. In addition, using photoelectron spectroscopy the excess electron binding energies have been measured for water[6] $(H_2O)_n^-$ (for n in the range 2 to 40) and alkali-halide clusters[10] [(Na_nCl_{n-1}) and (Na_nF_{n-1}), for $2 \leqslant n \leqslant 40$]. Furthermore, measurements and calculations of the optical spectra of alkali-halide clusters containing an excess electron are currently underway.[10(c),10(d),32(b)] The main observations pertaining to polar molecular clusters may be summarized as follows:

(1) The water dimer constitutes the smallest water cluster which attaches an electron, resulting in a weakly bound $(H_2O)_2^-$ state, with an estimated binding energy of ~ 17 meV (from field detachment experiments[3]) or ~ 30 meV (from photoelectron spectroscopy[6]).

(2) Strongly bound $(H_2O)_n^-$ clusters were observed[1–6] for $n \geqslant 11$, while for $(NH_3)_m^-$ the minimum cluster size detected[3] is ~ 35. In the case of water nonreactive electron localization in the clusters was experimentally documented to originate either from electron binding during the cluster nucleation process[1–4,6] or by electron attachment to preexisting clusters.[2,5]

(3) The stable $(H_2O)_n^-$ clusters ($n \geqslant 11$) are characterized by a large electron vertical binding energy which varies monotonically with cluster size[6] (-0.75 eV for $n = 11$ to -1.12 eV for $n = 19$).

On the theoretical front, early investigations of negatively charged clusters employed the methods of quantum chemistry for calculations of the electronic structure.[11,12,14,15] These calculations were limited to small clusters (up to ~ 10 water[11,12] or 3–5 alkali-halide molecules[14,15]) and were performed mostly for a restricted set of nuclear configurations. The recent development and application of the quantum-path integral molecular dynamics (QUPID) method,[18–20] the use[29,30,32,33] of the fast-Fourier-transform (FFT) technique for solution of the Schrödinger equation,[29,30,32–34,36] and the time-dependent self-consistent-field (TDSCF) method,[29,30,32–34,37,38] add a new dimension to the research of excess electron interaction with finite atomic and molecular aggregates.[19,20] Using these methods, in conjunction with well tested interatomic and intermolecular potentials[39–41] and pseudopotentials[16–26,34,35,42] for the description of the interaction of the excess electron with the atomic or molecular constituents of the cluster, yield a wealth of information about the equilibrium, finite tempera-

ture, energetics, structure,[17–35] and spectroscopy[29–33] of these systems and about the dynamics and mechanisms[32,33] of excess electron attachment, localization, migration, and solvation in clusters. The main findings from these studies pertaining to electron localization in polar molecular clusters may be summarized as follows:

(1) The localization mode of an excess electron in a polar molecular cluster depends on the cluster size and chemical constituents. For water clusters $(H_2O)_n^-$ in the size range $11 \leqslant n < 64$ the electron is relatively strongly bound in a surface state while for the larger clusters $(32 \leqslant n < 64)$ a gradual transition to internal solvation occurs.[23–27] Attachment of the excess electron to small clusters, $n < 10$ is in a diffuse weakly bound surface state.[17,24]

(2) The onset of stable well-bound electron attachment to ammonia clusters $(NH_3)_n^-$ occurs via internal localization, requiring $n \gtrsim 32$ molecules, and in contrast to the case of the water clusters is not preceded by well-bound surface states for smaller clusters.[28] The critical sizes for electron binding to water and ammonia clusters are in agreement with experimental observations.[1–6]

(3) The mechanism underlying the mode of localization (surface vs internal states) is a balance between the excess electron binding energy to the cluster and the energy associated with structural molecular reorganization in the cluster upon electron attachment. In the small and medium size water cluster regime $(n > 64)$ and for all sizes of ammonia clusters the cluster reorganization energy associated with the formation of an internal electron state is large compared to that which is gained via binding, resulting in surface localization of the excess electron. The transition to internal localization is associated with a reversal of the balance between binding and reorganization energies.

(4) The vertical binding energies calculated via the QUPID simulations[23–27] for surface states of $(H_2O)_n^-$ clusters in the range $12 \leqslant n \leqslant 18$ are in good agreement with those available from photoelectron spectroscopy experiments.[6]

(5) From analysis of QUPID simulation results[26,31] we conclude that the spectra of surface excess electron states in small- and medium-sized clusters $(H_2O)_n^-$ $(8 \leqslant n \leqslant 32)$ are characterized by bound–continuum transitions, and that the spectra of the energetically stable interior excess electron states in large $(H_2O)_n^-$ $(n \geqslant 64)$ clusters are characterized by bound–bound transitions.

(6) TDSCF simulations[30,32(b)] show that the electronic absorption spectrum in $(H_2O)_n^-$ $(n \geqslant 64)$ clusters, which is primarily associated with overlapping transition from (s-like) ground to the three (p-like) lowest excited states is only slightly sensitive to the cluster size. The calculated absorption peak predicted by these simulations is at 2.1 eV and has a width of ~ 1 eV, compared to the experimental results[43] for bulk water of 1.72 eV and 0.92, respectively.

(7) The smallest water cluster which attaches an excess electron is the water dimer. The binding energy is estimated to be between 3[17,24] and 25 meV,[24,29,30] depending on the nuclear configuration. At 20 K transitions between cluster configurations, characterized by low and high molecular dipole moments, with corresponding low and high excess electron binding energies, occur.[29,30]

In this paper we focus on studies of the smallest water cluster which binds an electron $[(H_2O)_2^-]$, using *ab initio* electronic structure calculations and quantum simulation methods. In addition to providing new information about the negatively charged water dimer, these comparative studies allow us to quantitatively assess the electron–molecule interaction pseudopotential[23–25] which we employ in the quantum simulations. In Sec. II we review briefly the quantum simulation methods and provide details pertinent to the *ab initio* quantum chemistry calculations. The results of our investigations are presented in Sec. III, and are summarized in Sec. IV.

II. METHODS AND INTERACTION POTENTIALS

A. Methods

In our theoretical studies of $(H_2O)_2^-$ we have used three methods:

(i) The quantum path-integral molecular dynamics (QUPID) method.

(ii) The fast-Fourier-transform (FFT) technique for solving the time-dependent Schrödinger equation, and in conjunction with the time-dependent self-consistent-field (TDSCF) method.

(iii) *Ab initio* quantum chemistry electronic structure methods for solving the many-electron Schrödinger equation for the $(H_2O)_2^-$ system, for selected nuclear configurations.

In the following we review these methods and the electron–water molecule pseudopotential which we employed in the quantum simulations.

1. The quantum path integral molecular dynamics (QUPID) method

The QUPID method rests on the Feynman path-integral formulation of quantum statistical mechanics,[44] and provides a convenient method for studies of the equilibrium, finite temperature properties of systems consisting of interacting quantum and classical degrees of freedom.[18,19] In this formulation the expression for the partition function Z for a system consisting of a quantum particle (mass m and coordinate $\mathbf{r}$) interacting with a set of N classical particles (whose phase-space trajectories are generated by classical equations of motion) via a potential $V(\mathbf{r}) = \Sigma_{j=1}^{N}(V(\mathbf{r},\mathbf{R}_j))$, is given as

$$Z_p = \left(\frac{mP}{2\pi\hbar^2\beta}\right)^{3P/2} \int d\mathbf{r}_1 \cdots d\mathbf{r}_P \, d\mathbf{R}_1 \cdots d\mathbf{R}_N \, e^{-\beta V_{\text{eff}}}, \tag{1a}$$

where

$$V_{\text{eff}} \equiv \sum_{i=1}^{P} \frac{mP}{2\hbar^2\beta^2}(\mathbf{r}_i - \mathbf{r}_{i+1})^2 + \frac{1}{P}\sum_{j=1}^{N}\sum_{i=1}^{P} V(\mathbf{r}_i,\mathbf{R}_j) + V_c(\mathbf{R}_1,\ldots,\mathbf{R}_N) \tag{1b}$$

and

$$Z \equiv \lim_{P\to\infty} Z_P. \tag{1c}$$

V_c is the interaction potential between the classical particles and $\beta = (k_B T)^{-1}$.

Equations (1) establish an isomorphism[44,45] between the quantum problem and a classical one in which the quantum particle is represented by a flexible periodic chain (necklace) of P pseudoparticles (beads) with nearest-neighbor harmonic interactions with a temperature-dependent spring constant, $Pm/\hbar^2\beta^2$. In practice, the finite value of P employed in the calculations is chosen to yield convergent results and depends upon the temperature and characteristics of the interaction potential V. In the case of $(H_2O)_2^-$ at $T = 20$ K a choice of $P = 16\,384$ proved to yield convergence.[24] The average energy of the system at equilibrium is given by

$$E = \frac{3N}{2\beta} + \langle V_c \rangle + K + \frac{1}{P}\left\langle \sum_{i=1}^{P} V(\mathbf{r}_i) \right\rangle, \tag{2a}$$

where

$$K = \frac{3}{2\beta} + \frac{1}{2P}\sum_{i=1}^{P}\left\langle \frac{\partial V(\mathbf{r}_i)}{\partial \mathbf{r}_i}\cdot(\mathbf{r}_i - \mathbf{r}_p)\right\rangle \tag{2b}$$

and the angular brackets indicate statistical averages over the probability distribution as defined by Eq. (1). The first two terms in Eq. (2a) are the mean kinetic and potential energies of the classical components of the system. The quantum particle kinetic energy estimator[46,47] K [Eq. (2b)] consists of the free particle term ($K_f = 3/2\beta$) and a contribution due to the interaction ($K_{\rm int}$). Finally, the last term in Eq. (2a) is the means potential energy of interaction between the quantum particle and the classical field.

The formalism described above is converted into a numerical algorithm by noting the equivalence[47] between the equilibrium statistical averages over the probability distribution given in Eq. (1) and sampling over phase space trajectories, generated by a classical Hamiltonian

$$H = \sum_{i=1}^{P}\frac{m^*\dot{\mathbf{r}}_i^2}{2} + \sum_{I=1}^{N}\frac{M_I\dot{\mathbf{R}}_I^2}{2} + \sum_{i=1}^{P}\left[\frac{Pm}{2\hbar^2\beta^2}(\mathbf{r}_i - \mathbf{r}_{i+1})^2 + \frac{V(\mathbf{r}_i)}{P}\right] + V_c(\mathbf{R}_1,\ldots,\mathbf{R}_N), \tag{3}$$

where m^* is an arbitrary mass, chosen such that the internal frequency of the necklace, $\omega = [mP/m^*\beta^2\hbar^2]^{1/2}$, will match the other frequencies of the system, and M_I is the mass of a classical particle.

Descriptions of the applications of the method to a wide variety of quantum many-body systems of chemical and physical interest can be found in Refs. 17–28.

2. The FFT technique and TDSCF method

The quantum time evolution in the FFT method is based on a repeated evaluation of the short-time propagation of the wave function (in real or imaginary time) according to[36]

$$\psi(\mathbf{r},t+\Delta t) = \exp\left[-\frac{i}{\hbar}(\hat{K}+\hat{V})\Delta t\right]\psi(\mathbf{r},t) = \exp\left[-\frac{1}{2}\frac{i}{\hbar}\hat{K}\Delta t\right]\exp\left[-\frac{i}{\hbar}\hat{V}\Delta t\right] \times \exp\left[-\frac{1}{2}\frac{i}{\hbar}\hat{K}\Delta t\right]\psi(\mathbf{r},t) + o[(\Delta t)^3], \tag{4}$$

where $\hat{K}$ and $\hat{V}$ are the kinetic and potential-energy operators, and an expansion in the plane-wave, free-particle, basis set

$$\psi(\mathbf{r},t+\Delta t) = \frac{1}{(2\pi)^3}\exp\left[-\frac{i}{2\hbar}\hat{K}\Delta t\right] \times \exp\left[-\frac{i}{\hbar}V(\mathbf{r})\Delta t\right] \times \int d^3k\, e^{-i\mathbf{k}\cdot\mathbf{r}}\exp\left[-\frac{i\hbar k^2}{4m}\Delta t\right] \times \int d_3r'\, e^{-i\mathbf{k}\cdot\mathbf{r}'}\psi(\mathbf{r}',t), \tag{5}$$

where m is the mass of the quantum particle and V is his interaction potential. The FFT algorithm is applied to the discretized version of Eq. (5) on a grid.

Using Eq. (4) for a fixed configuration of the nuclei and transforming to imaginary time, i.e., $t = -i\beta'$, propagation (using the FFT algorithm) from $\beta' = 0$ to a value β large enough so that the expectation value $E = \langle\psi(\beta)H\psi(\beta)\rangle/\langle\psi(\beta)\psi(\beta)\rangle$ converges to a constant value, allows determination of the ground-state energy E and corresponding ground-state wave function $\psi(\beta)$. Sequential determination of electronic excited states can be achieved via application of the above imaginary time propagation in conjunction with projection operators which project out of the initial wave function the previously determined lower states.[48,30,32,33,38,42]

In applying the FFT technique to the $(H_2O)_2^-$ system a grid of 64^3 points was used with the spacing Δ between grid points equal to $2a_0$. This large number of grid points (and the value of Δ) proved necessary due to the incompatibility between the nature of the diffuse excess electron wave function and the compact force field generated by the water molecules in this system.[24,30] As one of the criteria for the adequacy of the grid size we use the electron density-weighted grid-surface-to-volume ratio, defined as

$$\gamma = 1 - \Delta^3 \sum_{l,m,n=-N_g/2+2}^{N_g/2-1}\psi_{lmn}^*\psi_{lmn}, \tag{6}$$

where $\psi_{lmn} \equiv \psi(\mathbf{r}_{lmn},t)$ at the grid point (lmn) and the sum extends over all the grid points (N_g). For a uniform distribution of the electron density $\gamma = [N_g^3 - (N_g-2)^3]/N_g^3$, which for $N_g = 64$ yields 0.091. We thus require that in the calculations the value of γ will be much smaller than that value (when this condition is not satisfied the calculated energies depend on the size of the grid).

In the quantum-classical version of the TDSCF method [for a review see Ref. 36(d), for a critical study see Ref. 37(b), and for recent applications see Refs. 29, 30, 49, and

50] the coupled dynamical evolution of the quantum and classical degrees of freedom is described via the coupled equations

$$\frac{\partial\psi(\mathbf{r};\{\mathbf{R}\},t)}{\partial t} = -\frac{i}{\hbar}H(\mathbf{r};\{\mathbf{R}\})\psi(\mathbf{r};\{\mathbf{R}\},t), \tag{7a}$$

$$M_I\ddot{\mathbf{R}}_I = -\int d\mathbf{r}|\psi(\mathbf{r};\{\mathbf{R}\},t)|^2\frac{\partial}{\partial\mathbf{R}_I}V(\mathbf{r},\{\mathbf{R}\}) - \frac{\partial}{\partial\mathbf{R}_I}V_c(\{\mathbf{R}\}) \quad (I=1,...,N), \tag{7b}$$

$$H(\mathbf{r};\{\mathbf{R}\}) = H_0(\mathbf{r}) + V(\mathbf{r},\{\mathbf{R}\}), \tag{7c}$$

where $\{\mathbf{R}\}$ denotes the collection of vector positions of the N atomic (classical) constituents of masses M_I, H_0 is the Hamiltonian of the isolated quantum subsystem, $V(\mathbf{r},\{\mathbf{R}\})$ is the interaction potential between the quantum and classical degrees of freedom and $V_c\{\mathbf{R}\}$ the interatomic potential. In this approximation the classical subsystems evolves in the quantum-averaged interaction potential $\langle V\rangle$ [integral on the right-hand side of Eq. (7b)] and the classical interaction $V_c(\{\mathbf{R}\})$.

For many situations, where the adiabatic (Born–Oppenheimer) approximation applies, propagation of the classical subsystems can be performed on a single chosen electronic energy surface, by restricting the electronic wave function to remain in that chosen state throughout the simulation.[29,30,32,33,49] For $(H_2O)_2^-$, however, this adiabatic simulation method cannot be applied since the binding energy of the electron (in the range of ~3–30 meV, depending on the molecular configuration of the cluster[24,30]) is of the same order as the energy of the lowest intermolecular vibrational mode of the neutral dimer. Therefore, for this system the full real-time evolution was simulated in the TDSCF approximation.[29,30(a)] It should be noted that, as is usual with Hartree and Hartree–Fock type approximations, the use of the self-consistent-field approximation in the present context can be justified only *a posteriori* by comparing to results obtained by other methods.

3. Ab initio calculations

For specific nuclear configurations of $(H_2O)_2^-$, selected from the equilibrium ensemble generated via the QUPID method (see Sec. II A 1), we have performed first principle electronic structure calculations. In these investigations the Gaussian 86 *ab initio* computer codes[51] were used. A very good basis set for the water molecules was selected and then supplemented with a large diffuse set located at the midpoint between the two oxygens. The basis set selected is the most recent one proposed by Clementi and Habitz.[52] It is very similar to the modified MCY basis[53] (MCY′) studied by Newton and Kestner[54,55] in their analysis of the water dimer. This basis set yields a very good value for the total energy of the water molecule, −76.056 035 hartree, which is very close to the Hartree–Fock limit. The optimal OH bond length and HOH angle are 0.9461 a_0 and 105.56, respectively, at the Hartree–Fock level. At this level the dipole moment of the H_2O molecule, corresponding to the optimal SCF geometry is 0.7785 $e\,a_0$ (1 $e\,a_0$ = 2.524 D).

For the diffuse basis set representing the loosely attached excess electron we took the basis functions suggested by Chipman[12] in his paper on the negatively charged water dimer. It consists of a set of seven s and seven p orbitals which have exponents which decrease by a factor of 8 from one to another. They do indeed span the space needed as in all of the runs to be discussed the largest coefficients are found for basis functions in the middle of the set. The largest exponent is 0.262 while the smallest is 0.000 001. In order to make the calculations manageable beyond the Hartree–Fock limit where the above set can create instabilities due to the many small eigenvalues, another set of calculations were made using the contraction of the highest occupied molecular orbital (HOMO) optimized for the negative water dimer of interest. That set is referred to as the contracted set in the tables to follow (see Sec. III).

B. The electron–molecule pseudopotential

A key issue in modeling the system by the one-electron QUPID and TDSCF methods is the choice of interaction potentials. Fortunately, for small water clusters, interaction potential functions that provide a satisfactory description for a range of properties are available. We have used the RWK2-M model[39] for the intra- and interwater interactions. Less is known about the electron–water interaction. We have constructed[23–25] a pseudopotential that consists of Coulomb, polarization, exclusion, and exchange contributions:

$$V(\mathbf{r}_e,\mathbf{R}_0,\mathbf{R}_1,\mathbf{R}_2) = V_{\text{Coul}} + V_p + V_e + V_x. \tag{8a}$$

The positions of the oxygen and hydrogen nuclei of the water molecule are given by $(\mathbf{R}_0,\mathbf{R}_1,\mathbf{R}_2)$, and $\mathbf{r}_e$ is the position of the electron.

The Coulomb interaction is

$$V_{\text{Coul}}(\mathbf{r}_e,\mathbf{R}_0,\mathbf{R}_1,\mathbf{R}_2) = -\sum_{j=1}^{3} q_j e/\max(|\mathbf{r}_e-\mathbf{R}_j|,R_{cc}), \tag{8b}$$

where $\mathbf{R}_3 = \mathbf{R}_0 + (\mathbf{R}_1+\mathbf{R}_2-2\mathbf{R}_0)\delta$ is the position of the negative point of charge of the RWK2-M model; q_1 and $q_2 = 0.6\,e$, $q_3 = -1.2\,e$, and $\delta = 0.221\,875\,6$. The values of q_j and δ were chosen[39] to give a good representation of the dipole and quadrupole moments of the water monomer. The cutoff radius R_{cc} was taken to be 0.5 a_0, and the results are insensitive to the precise value of R_{cc}.

The polarization interaction is given by

$$V_p(\mathbf{r}_e,\mathbf{R}_0) = -0.5\alpha e^2/(|r_e-R_0|^2+R_p^2)^2, \tag{8c}$$

where $\alpha = 9.7446$ a.u. is the spherical polarizability of the water molecule. The form of V_p and the value of $R_p = 1.6\,a_0$ were chosen to fit approximately the adiabatic polarization potential as calculated by Douglass *et al.*[56] for an approach of the electrons along the H–O–H bisector (see Table 7 and Fig. 2 in Ref. 56).

The exclusion V_e and the exchange V_x contributions both require the electron density $\rho(\mathbf{r},\mathbf{R}_0,\mathbf{R}_1,\mathbf{R}_2)$ of the water molecule. We find that a reasonable fit to the calculated electron density,[57] in the regions of importance, is provided by

$$\rho(\mathbf{r},\mathbf{R}_0,\mathbf{R}_1,\mathbf{R}_2) = 8a_0^{-3}\, e^{-3|\mathbf{r}-\mathbf{R}_0|/a_0} + a_0^{-3} \times \sum_{j=1}^{2} e^{-3|\mathbf{r}-\mathbf{R}_j|/a_0}. \quad (8d)$$

The repulsion, due to the exclusion principle, is modeled as a "local kinetic energy term."[58] This contribution accounts for the orthogonality constraint between the wave function of the excess electron and the valence molecular electronic orbitals. In our calculation this contribution is modeled as

$$V_e(\mathbf{r}_e,\mathbf{R}_0,\mathbf{R}_1,\mathbf{R}_2) = 0.5e^2a_0(3\pi^2\rho)^{2/3}. \quad (8e)$$

Finally, the exchange contribution, which is a consequence of the antisymmetrization of the wave function, is modeled within the local exchange approximation[59] by

$$V_x(\mathbf{r}_e,\mathbf{R}_0,\mathbf{R}_1,\mathbf{R}_2) = -\alpha_x e^2(3\pi^2\rho)^{1/3}/\pi. \quad (8f)$$

The parameter α_x was taken to be $\alpha_x = 0.3$ in order to obtain good agreement between our simulation results and the SCF results of Rao and Kestner[11(b)] for $(H_2O)_8^-$ at a fixed octahedral configuration of the water molecule.

A detailed analysis of this pseudopotential, and its application in studies of electron localization in clusters can be found elsewhere.[25,26]

III. RESULTS

The energetics and dynamics of the negatively charged water dimer, $(H_2O)_2^-$, have been the subject of recent experimental[3,6] and theoretical[17,24,29,30(a)] studies. Using the QUPID method (see Sec. II) we have performed simulations at $T = 20$ K (employing 16 384 beads) of this system.[24] In these studies it was found that while in equilibrium the electron adiabatic binding energy (EABE) (i.e., the energy of the electron interacting with the molecules plus the cluster reorganization energy, see below) is the smallest for a nuclear configuration of the negatively charged water dimer which is close to the optimal configuration of the neutral dimer (see the Appendix), other, metastable, configurations occur. In particular, these configurations correspond to a libration of one of the water molecules [the acceptor molecule, see Fig. 1 and Fig. 2(a)], resulting in an increase in the cluster molecular dipole and consequently an increase in the magnitude of the electron vertical binding energy which is accompanied by a contraction of the spatial extent of the electron distribution [compare the high-dipole and low-dipole configurations of $(H_2O)_2^-$, obtained from QUPID simulations,[24] shown in Figs. 2(a) and 2(b), respectively]. We remark, that for the high-dipole [Fig. 2(a)] configuration of the $(H_2O)_2^-$ cluster EABE is larger than for the low-dipole

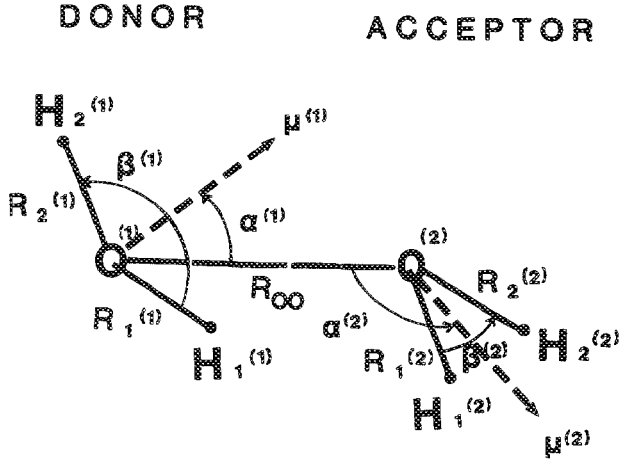

FIG. 1. A schematic representation of the geometry of $(H_2O)_2$. The atoms belonging to the donor and acceptor molecules are distinguished by the superscripts, (1) and (2), respectively. The distance between the oxygens is R_{OO}. $R_j^{(i)}$ (for $i = 1,2$ and $j = 1,2$) are the O–H bond lengths in the dimer molecules. $\alpha^{(j)}$ ($j = 1,2$) is the angle between the molecular dipole, $\mu^{(j)}$ and the $O^{(1)}$–$O^{(2)}$ axis. $\alpha^{(2)}$ equals to zero for $\mu^{(2)}$ parallel to the $O^{(1)}$–$O^{(2)}$ axis and is traversed anticlockwise. The $H_1^{(j)}$–$O^{(j)}$–$H_2^{(j)}$ ($j = 1,2$) angle is denoted by $\beta^{(j)}$.

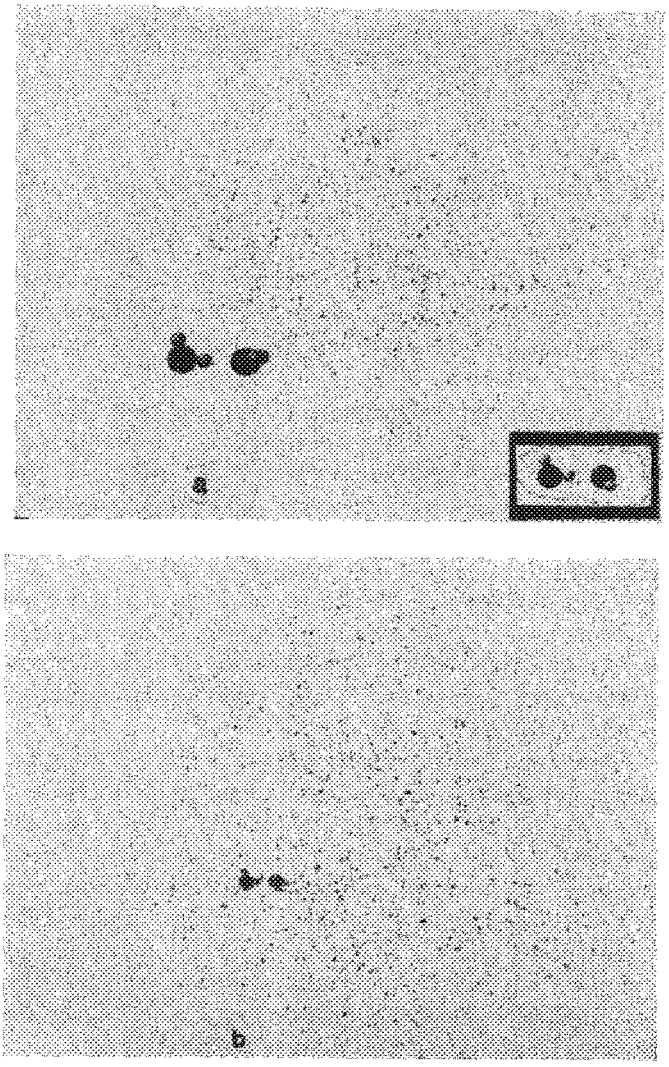

FIG. 2. Representative configurations of $(H_2O)_2^-$ from QUPID simulations (Ref. 24) at 20 K: (a) The high-dipole (HD) configuration. In the inset the configuration of a neutral water dimer is shown. (b) The equilibrium, low-dipole (LD) configuration. Large dark balls represent the oxygen atoms and the smaller grey ones represent the hydrogens. The dark dots represent the beads, i.e., the excess electron density distribution corresponds to the density of the dark dots.

TABLE I. QUPID and FFT results for LD, ID, and HD, $(H_2O)_2^-$ configurations. The results for the LD configuration are averaged over the equilibrium ensemble generated at 20 K via QUPID simulations (Ref. 24). The values in parentheses are the standard deviations. For the ID and HD configurations the results calculated via the FFT method are for the representative configurations selected from the QUPID simulations (Ref. 24). $\phi^{(1)}$, $\phi^{(2)}$, and V_c are the intramolecular, intermolecular, and total potential energies of the molecular cluster. E_c is the molecular cluster reorganization energy $\{E_c = V_c[(H_2O)_2^-] - V_c[(H_2O)_2]\}$. V and K_e are the excess electron-cluster interaction potential energy and excess electron kinetic energies, respectively. EVBE $= V + K_e$ is the excess electron vertical binding energy, and EABE $=$ EVBE $+ E_c$ is the excess electron adiabatic binding energy. μ is the total molecular dipole of the dimer (in units of $e\,a_0 = 2.524$ D). Energies in units of Hartree (1 hartree $= 27.21$ eV) and length in units of Bohr radius, a_0.

Configuration	LD[a]	ID	HD
$\phi^{(1)}$	6×10^{-4} (3×10^{-4})	3.77×10^{-4}	7.166×10^{-4}
$\phi^{(2)}$	-1×10^{-2} (3×10^{-4})	-9.551×10^{-3}	-9.009×10^{-3}
V_c	-9.4×10^{-3}	-9.18×10^{-3}	-8.29×10^{-3}
E_c	0.0	0.61×10^{-3}	1.5×10^{-3}
V	-0.8×10^{-3} (1×10^{-4})	-0.85×10^{-3}	-2.38×10^{-3}
K_e	0.7×10^{-3} (1.4×10^{-3})	0.61×10^{-3}	1.91×10^{-3}
EVBE	-1×10^{-4} (1.4×10^{-3})	-2.5×10^{-4}	-4.7×10^{-4}
EABE	-0.1×10^{-3}	0.36×10^{-3}	1.03×10^{-3}
μ	1.02 (0.09)	1.283	1.513

[a] From QUPID simulations, see Ref. 24.

[Fig. 2(b)] configuration (see Table I), reflecting the possible metastability of the high-dipole configuration due to the cluster reorganization energy involved in the transition to such configurations [indeed in Ref. 30(a) we have shown that the high-dipole configuration does exist for finite time intervals along the trajectory of the $(H_2O)_2^-$ cluster at 20 K].

More recently, the energetics and dynamics of $(H_2O)_2^-$ was investigated[29,30] via real-time dynamic simulations, within the TDSCF approximation, at 20 K (using a 16^3 grid with a spacing between grid points equal to $9\,a_0$). Analysis of the system trajectories revealed dynamical nuclear structural transitions (on the time scale of <1 ps) between low-dipole and high-dipole configurations, similar to those observed in the QUPID simulations (see Fig. 2), accompanied by corresponding variations in the electron binding (fluctuating between -3 and -22 meV) and cluster molecular energies [see Fig. 14 in Ref. 30(a)].

Based on these results, we present in the following detailed comparative calculations of the energetics of $(H_2O)_2^-$ using QUPID, FFT, and *ab initio* calculations. For the purpose of this study we selected three representative nuclear configurations from the equilibrium ensemble generated via the QUPID simulations[24] at 20 K: (i) a low-dipole (LD) configuration, $\langle\mu\rangle = 1.02\,e\,a_0$, in which the nuclear configuration is similar to that of the neutral dimer [see Fig. 2(b)]; (ii) a high-dipole (HD) configuration, $\mu = 1.513\,e\,a_0$ [see Fig. 2(a)]; and (iii) an intermediate-dipole (ID) configuration, $\mu = 1.283\,e\,a_0$. Details of the geometry of the selected configurations are given in the Appendix. We should emphasize that the ID and LD configurations selected for the purpose of this study are not the average configurations of the corresonding metastable states of $(H_2O)_2^-$. Rather, they are individual configurations, selected from the equilibrium ensemble generated via the QUPID simulations.

The excess electron binding energy for the high and intermediate dipole configurations was determined using the FFT method (via imaginary-time propagation, see Sec. II) employing a large grid, i.e., $64\times64\times64$, with a spacing of $2a_0$ between grid points. Such large grids proved to be necessary due to the diffuse character of the ground state excess electron wave function (see Figs. 3 and 4, for the ID and HD configurations). For the HD configuration γ [see Eq. (6)] is equal to 0.016 (recall that for a uniform distribution $\gamma = 0.091$) and for the ID configuration it is somewhat higher, i.e., $\gamma = 0.043$. Thus in comparing the results with those obtained via *ab initio* calculations (see below) one is reminded that the results obtained by the FFT method for the ID configuration are less accurate than those obtained for the HD configuration. For the LD configuration, the diffuseness of the electron distribution prohibits calculations on the above grid. Therefore, for this cluster configuration we quote our previous equilibrium average results obtained via QUPID simulations at 20 K.

From Table I we observe that the magnitude of vertical binding energy of the excess electron (EVBE) increases monotonically with increase in the total molecular dipole of the cluster (~ -3.0, -7.0, and -13.0 meV for the LD, ID, and HD configurations, respectively). The equilibrium averaged LD configuration of $(H_2O)_2^-$ does not differ significantly from that of the neutral dimer $(H_2O)_2$ (see the Appendix), and thus the cluster reorganization energy E_c vanishes. However, the transition from the LD to the HD nuclear configurations is accompanied by an increase (to a smaller absolute value) in the cluster potential energy (V_c), mostly due to a weaker intermolecular interaction ($\phi^{(2)}$), resulting in $E_c > 0$ and thus a net increase in the adiabatic electron binding energy, EABE $=$ EVBE $+ E_c$.

Contours of the excess electron ground state wave functions obtained via the FFT calculations for the ID and HD configurations are shown in Figs. 3 and 4, respectively [compare also Fig. 4(a) to the electron density distribution ob-

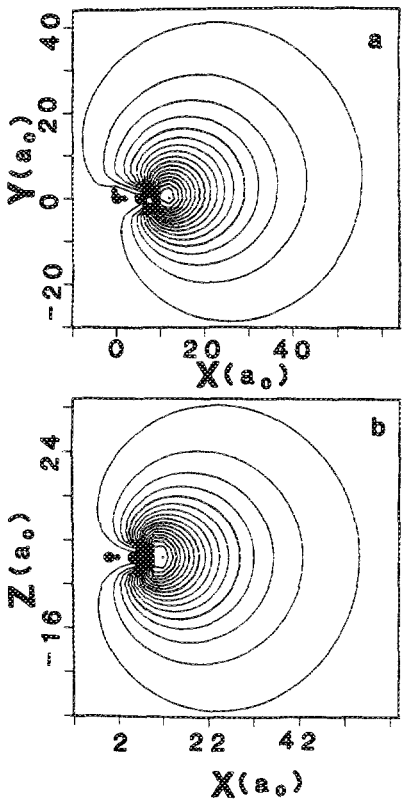

FIG. 3. Contour plots of the excess electron distribution for the *intermediate-dipole* (*ID*) configuration of $(H_2O)_2^-$, obtained via the FFT method. (a) In the plane containing the two oxygens and the nondonated hydrogen of the donor molecule. The increment δ between contour lines is 1×10^{-6} a_0^{-3} and the maximum contour corresponds to 18×10^{-6} a_0^{-3}. (b) In the plane which contains the oxygens and is normal to that shown in (a). $\delta=1\times10^{-6}$ a_0^{-3} and the maximum contour corresponds to 18 a_0^{-3}.

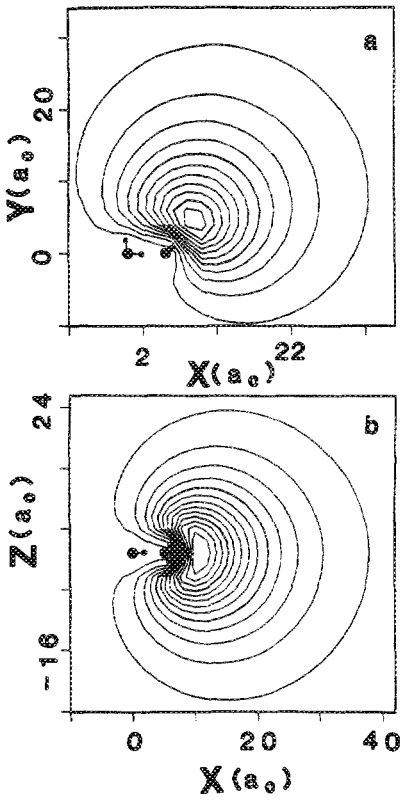

FIG. 4. Contour plots of the excess elecron distribution for the *high-dipole* (*HD*) configuration of $(H_2O)_2^-$, obtained via the FFT method. (a) In the plane containing the two oxygens and the nondonated hydrogen of the donor molecule. The increment δ between contour lines is 5×10^{-6} a_0^{-3} and the maximum contour correspond to 55×10^{-6} a_0^{-3}. (b) In the plane which contains the oxygens and is normal to the plane shown in (a). $\delta=2.5\times10^{-6}$ a_0^{-3} and the maximum contour corresponds to 32.5×10^{-6} a_0^{-3}.

tained via the QUPID method shown in Fig. 2(a)]. As seen from these figures while for the LD configuration [Fig. 2(b)] the electron is distributed around the molecules of the cluster, as the dipole of the molecular configuration increases the electron distribution focuses more in the direction of the molecular dipole and its spatial extent is reduced, correlating with the increase in the excess electron binding energy.

The relative contributions of the various terms in the electron–molecule pseudopotential [see Eqs. (8a)–(8f)] to the excess electron potential energy are given in Table II. We note that for all three configurations the magnitude of the contribution due to the Coulomb term V_{Coul} is the largest. The increase in the relative contributions from the other terms in V upon increase of the dipole of the nuclear configuration, correlates with the increase in binding (see Table I) which is accompanied by a more compact character of the excess electron distribution (compare Figs. 2–4). Thus in the ID and HD configurations the centroid of the electron distribution is closer to the center of mass of the dimer, resulting in larger (absolute) values of the polarization, exclusion, and exchange contributions, than in the LD configuration.

We turn next to the results obtained from the *ab initio* calculations (see Sec. II). Calculations were performed for the above ID and HD configurations and for the negatively charged dimer in the optimal molecular configuration of the neutral dimer. The nuclear coordinates of the water molecules in the ID and HD configurations (see the Appendix for details), which were obtained from the QUPID simulations[24] and used here for the purpose of comparison with the FFT calculations discussed above, do not correspond to the optimal OH bond length and HOH angle of the water molecule from *ab initio* calculations. However, the differences are

TABLE II. Relative contributions of the Coulomb, polarization, exclusion, and exchange terms in the electron–water interaction pseudopotential to the total potential energy of an excess electron in $(H_2O)_2^-$.

Configuration	LD[a]	ID	HD
$V_{\text{coul}}/\lvert V\rvert$	−0.919	−0.916	−0.919
$V_p/\lvert V\rvert$	−0.081	−0.154	−0.161
$V_e/\lvert V\rvert$	0.026	0.182	0.206
$V_x/\lvert V\rvert$	−0.025	−0.112	−0.126

[a] From QUPID simulations, see Ref. 24.

TABLE III. *Ab initio* results for the HD water dimer configuration. Energies of the highest occupied orbital (HOMO) in $(H_2O)_2^-$ and lowest unoccupied orbital (LUMO) in $(H_2O)_2$, unrestricted Hartree-Fock (UHF) total energies for the neutral and negatively charged dimers and total energies which include correlation energy corrections via second-order perturbation theory (MP2). Values are given for calculations using the full uncontracted diffuse basis set, as well as those for calculations using contracted *s* and *p* diffuse functions in the outer orbital (HOMO) optimized for the negatively charged dimer (values in parentheses). The binding energies of the excess electron, EVBE, estimated via Koopman's theorem (under orbital energy) and from the difference of total energies of the charged and neutral dimers (under UHF and MP2) are given. Energies in units of Hartree.

	Orbital energy	*E*(UHF)	Correlated energy (MP2)
$(H_2O)_2^-$	-4.9×10^{-4}	$-152.113\,71$	
	(-4.9×10^{-4})	$(-152.113\,12)$	$(-152.552\,81)$
$(H_2O)_2$	-4.5×10^{-4}	$-152.113\,24$	$-152.555\,88$
	(-4.4×10^{-4})	$(-152.112\,65)$	$(-152.552\,06)$
EVBE	-4.5×10^{-4}	-4.7×10^{-4}	
	(-4.4×10^{-4})	(-4.6×10^{-4})	(-7.5×10^{-4})

not large, since for the optimal singie molecule H_2O configuration the value obtained via the *ab initio* calculations is 1.965 D while for the configurations selected from the QUPID simulations the values obtained for the dipole moments of the individual H_2O molecules are 2.04 and 2.01 D for the HD configuration and 2.01 and 1.98 D for the ID configuration, respectively.

Results for the HD and ID configurations of $(H_2O)_2^-$ and $(H_2O)_2$ are given in Tables III and IV. The verical binding energy of the excess electron, EVBE, is calculated both via Koopman's theorem [i.e., the energy of the lowest unoccupied molecular orbital (LUMO) in the neutral system, thus assuming that upon attachment of the excess electron the other orbitals are not affected] and as the difference between the total energies of the negatively charged and neutral systems (thus allowing for relaxation of the electronic orbitals upon excess electron attachment). In addition to results of calculations employing the full basis set, results of calculations performed with a contraction of the highest molecular orbital (HOMO), optimized for the negatively charged water dimer of interest, are given (in parentheses).

The electron densities corresponding to the HD and ID configurations of $(H_2O)_2^-$ are shown in Figs. 5 and 6, respectively. In these contour plots, only the most diffuse functions were plotted, and we have deliberately suppressed the rapid oscillations associated with the requirement of orthogonality to the inner atomic orbitals near the nuclei. The close agreement between these results and those obtained via the FFT method in conjunction with the one-electron pseudopotential (see Figs. 4 and 3 for the HD and ID configurations, respectively) is evident.

The binding energies, EVBE, obtained via the *ab initio* calculations (see Tables III and IV) and those obtained for the same nuclear configurations, using the FFT method and employing the pseudopotential for the excess electron interaction with the water molecules (see values of EVBE in Table I), compare favorably, particularly in view of the simplicity of the pseudopotential used in the latter calculations

TABLE IV. *Ab initio* results for intermediate-dipole (ID) water dimer configuration. Energies of the highest occupied orbital (HOMO) in $(H_2O)_2^-$ and lowest unoccupied orbital (LUMO) in $(H_2O)_2$, unrestricted Hartree-Fock (UHF) total energies for the neutral and negatively charged dimers and total energies which include correlation energy corrections via second-order perturbation theory (MP2). Values are given for calculations using the full uncontracted diffuse basis set, as well as those for calculations using contracted *s* and *p* diffuse functions in the outer orbital (values in parentheses). The binding energies of the excess electron, EVBE, estimated via Koopman's theorem (under orbital energy) and from the difference of total energies (under UHF and MP2) are given. Energies in units of Hartree.

	Orbital energy	*E*(UHF)	Correlated energy (MP2)
$(H_2O)_2^-$	-1.9×10^{-4}	$-152.116\,06$	
	(-2.1×10^{-4})	$(-152.115\,46)$	$(-152.554\,47)$
$(H_2O)_2$	-1.7×10^{-4}	$-152.115\,88$	$-152.557\,89$
	(-1.9×10^{-4})	$(-152.115\,26)$	$(-152.554\,15)$
EVBE	-1.7×10^{-4}	-1.8×10^{-4}	
	(-1.9×10^{-4})	(-2.0×10^{-4})	(-3.2×10^{-4})

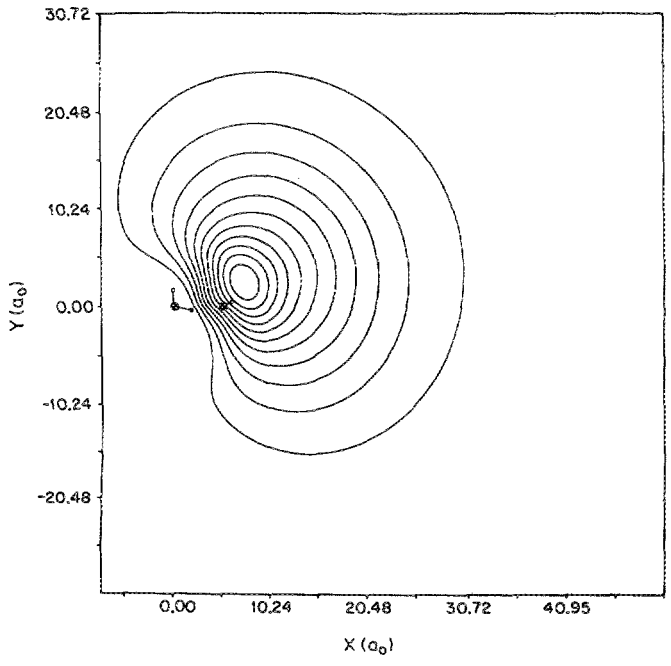

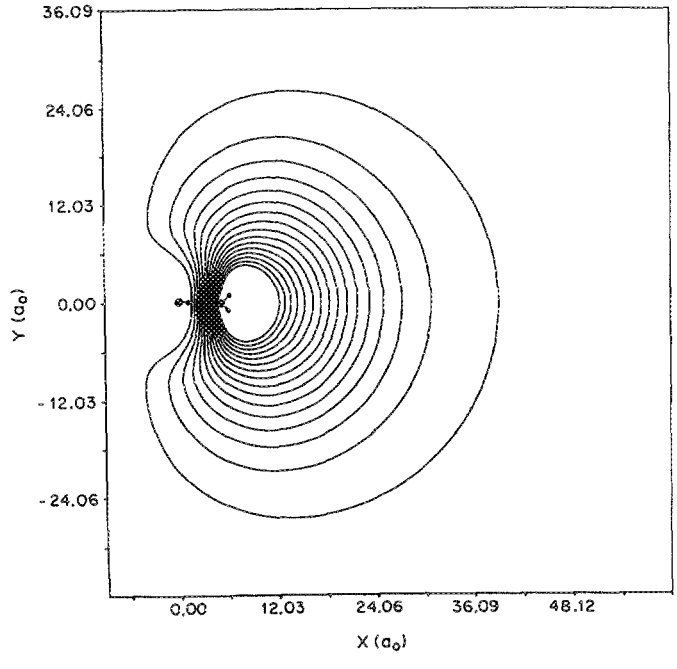

FIG. 5. Contour plots, of the highest occupied orbital in $(H_2O)_2^-$ in the *high-dipole* (*HD*) configuration obtained via *ab initio* calculations. (a) In the plane containing the two oxygens and the nondonated hydrogen of the donor molecule. The increment δ between contour lines is $5\times10^{-6}\,a_0^{-3}$ and the maximum contour corresponds to $55\times10^{-6}\,a_0^{-3}$. (b) In the plane containing the two oxygens and normal to that shown in (a). $\delta = 2.5\times10^{-6}\,a_0^{-3}$ and the maximum contour corresponds to $40\times10^{-6}\,a_0^{-3}$.

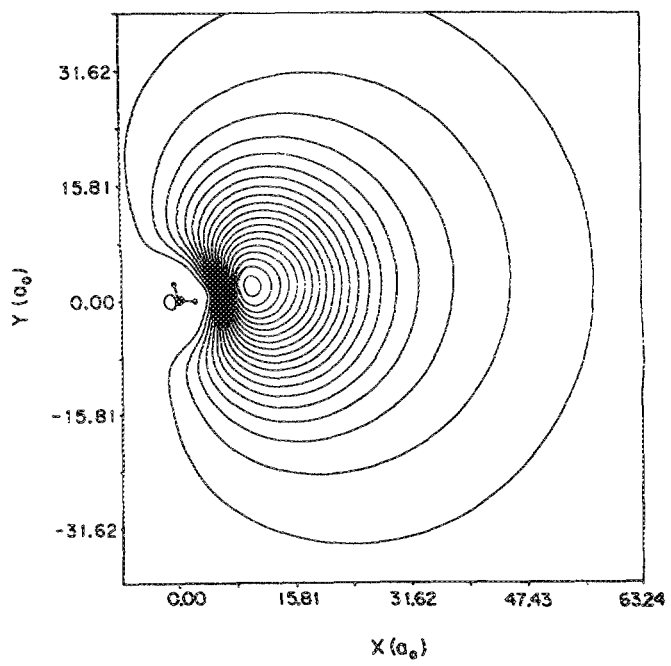

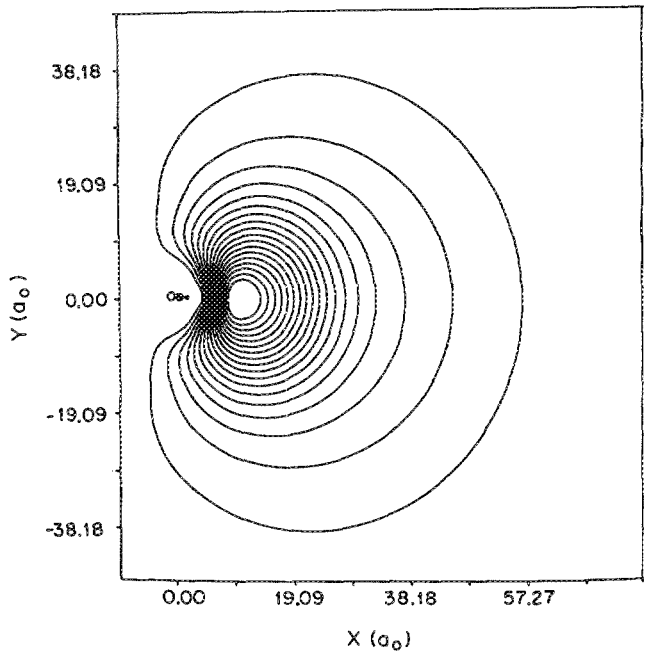

FIG. 6. Contour plots, of the highest occupied orbital in $(H_2O)_2^-$ in the *intermediate-dipole* (*ID*) configuration obtained via *ab initio* calculations. (a) In the plane containing the two oxygens and the nondonated hydrogen of the donor molecule. $\delta = 1\times10^{-6}\,a_0^{-3}$ and the maximum contour corresponds to $20\times10^{-6}\,a_0^{-3}$. (b) In the plane containing the two oxygens and normal to that shown in (a). $\delta = 1\times10^{-6}\,a_0^{-3}$ and the maximum contour corresponds to $18\times10^{-6}\,a_0^{-3}$.

(see Sec. II). Consequently, these results further substantiate our belief that the pseudopotential which we have constructed and employed in our studies of the energetics, dynamics, and spectroscopy of electron solvation in water clusters of varying sizes, provides a rather accurate representation of the interaction between the excess electron and the water molecules.

Comparison between the values for the binding energy, EVBE, estimated via Koopman's theorem and those determined as the total energy difference (compare values in the

TABLE V. Energy of the lowest unoccupied orbital (LUMO) in the neutral and total unrestricted Hartree–Fock (UHF) energies for the negatively charged and neutral dimers, calculated for the optimal neutral dimer configuration, using the large, uncontracted basis set. The excess electron binding energy, EVBE, is obtained via Koopman's theorem (under orbital energy) and as the difference between the total energies (under UHF). Energies in units of Hartree.

	Orbital energy	E(UHF)
$(H_2O)_2^-$	...	$-152.115\,61$
$(H_2O)_2$	-2×10^{-5}	$-152.115\,59$
EVBE	-2.0×10^{-5}	-2.0×10^{-5}

first and second columns of Tables III and IV) indicate close agreement between these two methods of estimating EVBE. However, the energies of the LUMO in the neutral dimer and HOMO in the negatively charged cluster differ somewhat (see first columns in Tables III and IV) thus indicating that even for these diffuse orbitals, estimates of the binding energy on the basis of Koopman's theorem should be viewed with caution.

We have also attempted to estimate the correlation corrections to the energy via the Møller–Plesset second-order perturbation theory[60] (MP2). Our results (see third column in Tables III and IV, under MP2) indicate the range and possible significance of correlation effects in these systems (e.g., for the HD water–dimer configuration the correlation correction to EVBE is ~60% of the value of this quantity calculated without correlations). However one should note that the MP2 method tends to overestimate the correlation energy corrections. Therefore one is cautioned against drawing from the above results definite conclusions concerning the magnitude of correlation contributions.

Finally, we remark on results of *ab initio* calculations, using the large uncontracted basis set, for $(H_2O)_2^-$ in a nuclear configuration corresponding to the optimal geometry of the neutral dimer for the basis set used.[54,55] In this geometry, which is close to the experimentally determined[61] configuration for $(H_2O)_2$, the distance between the oxygens is 5.631 a_0 and the tilt angle between the molecular plane of the acceptor molecule and the oxygen–oxygen axis ($\alpha^{(2)}$ angle in Fig. 1, see the Appendix) is 140°. The molecular dipole moment for this configuration is 1.90 D (i.e., 0.753 $e\,a_0$). The results are given in Table V for EVBE, obtained via Koopman's theorem and as the difference between the total energies of the neutral and negatively charged dimers. The value thus obtained for the electron binding energy is -2.0×10^{-5} hartree = 0.54 meV (compare to ~0.2 meV obtained by Chipman[12] for a slightly different geometry, for which the dipole moment was 2.05 D).

IV. SUMMARY

The main objective of our investigation was to compare the energetics and excess electron distribution in $(H_2O)_2^-$, calculated via quantum simulations (QUPID and FFT) and employing a one-electron pseudopotential for the interaction between the water molecules and the excess electron, with those obtained via *ab initio* calculations, for selected nuclear configurations of the dimer.

Previous QUPID[17,24] and TDSCF[29,30] simulations at 20 K have shown that the *equilibrium averaged* nuclear configuration (referred to as the low-dipole configuration) of the $(H_2O)_2^-$ cluster is very close to that of the neutral dimer, characterized by an excess electron vertical binding energy of ~3 meV and a negative adiabatic electron binding energy (see values for EVBE and EABE under LD in Table I). Furthermore, certain of these simulations[24,29,30] have provided evidence that the equilibrium ensemble at 20 K consists also of nuclear configurations of $(H_2O)_2^-$ which are characterized by large distortions of the intermolecular orientations as compared to that of the neutral dimer, leading to larger values of the total molecular dipole of the cluster and consequently resulting in stronger binding of the excess electron (the occurrence of these configurations and their contribution to the equilibrium ensemble average are reflected in the large standard deviation of the equilibrium averaged result; see values under LD in Table I). Estimates of the excess electron binding energy in $(H_2O)_2^-$, obtained via field detachment[3] and photoelectron spectroscopy[6] (yielding ~17 and ~30 meV, respectively), provide further evidence for the occurrence of such high-dipole configurations.

As stated above, in the present study we focused on comparative investigations of the energetics and excess electron distributions corresponding to several molecular configurations of $(H_2O)_2^-$. To this end we have selected individual typical configurations out of the equilibrium ensemble generated via the QUPID simulations.[24] The satisfactory agreement between the binding energies and excess electron distributions calculated by us using the FFT method in conjunction with a one-electron pseudopotential (see Sec. II) and those obtained via *ab initio* calculations, provides further support for the adequacy of the pseudopotential which we have constructed[25] and employed in extensive studies[23–33] of excess electron states in polar molecular clusters. Furthermore these comparative studies provide detailed information concerning the energetics and electronic distribution in $(H_2O)_2^-$, and their dependence on the intermolecular configuration.

In confronting our theoretical results with the experimental observations[3,6] we should remark that for the high-dipole (HD) molecular configuration which we have selected, the calculated values for the vertical binding energy of the excess electron are close, although somewhat higher (lower in absolute magnitude), to those obtained experimentally. Moreover, from a comparison between the calculated values of EVBE for the various cluster configurations and those determined from experiments it appears that the high-dipole (HD) cluster configurations of $(H_2O)_2^-$ (i.e., those configurations corresponding to stronger binding of the excess electron) are prevalent in the supersonic expansion beams interrogated experimentally.

ACKNOWLEDGMENTS

This research was supported by the U. S. DOE under Grant No. FG05-86ER45234 (to U.L.), and FG05-87ER13674 (to N.K.), the U.S.–Israel Binational Science Foundation Grant No. 85-00361 (to J.J. and U.L.), and the Commission for Basis Research of the Israel Academy of Science (to A.N.).

TABLE VI. Structural characteristics of the water dimer configurations studied. For definitions of the geometrical parameters see Fig. 1. The geometrical parameters for the LD configuration of $(H_2O)_2^-$ are averaged over the equilibrium ensemble generated via QUPID simulations (Ref. 24) at 20 K. The values for the intermediate and high-dipole configurations (ID and HD, respectively) of $(H_2O)_2^-$ are those of individual configurations selected from the QUPID simulations (Ref. 24). For the neutral clusters, equilibrium averaged values at 20 K [for $(H_2O)_2$] as well as values for minimum energy configurations at 0 K are given. Standard deviations are given in parentheses. Distances in a_0 and dipole moments in $e\,a_0$ ($1e\,a_0 = 2.524$ D).

Configuration	LD[a]	ID	HD	H_2O[b]	$(H_2O)_2$[c]	$(H_2O)_2$ ($T = 20$ K)[d]
R_{00}	5.215 (0.055)	5.270	5.119	···	5.187	5.207 (0.052)
$R_1^{(1)}$	1.851 (0.012)	1.835	1.848	1.809	1.849	1.848 (0.013)
$R_2^{(1)}$	1.800 (0.015)	1.817	1.806	1.809	1.807	1.807 (0.011)
$R_1^{(2)}$	1.817 (0.009)	1.832	1.795	···	1.815	1.815 (0.012)
$R_2^{(2)}$	1.817 (0.012)	1.804	1.823	···	1.815	1.815 (0.010)
$\alpha^{(1)}$	52° (2.5°)	52.8°	47.5°	···	53.8°	54° (2°)
$\beta^{(1)}$	103.8° (1.6°)	103.8°	101.9°	104.5°	104.1°	104.2° (1.4°)
$\alpha^{(2)}$	137 (9°)	171.7°	220.8°	···	126.6°	130.2° (10°)
$\beta^{(2)}$	104.0° (1.3°)	105.2°	102.9°	···	104.5°	104.6° (1.3°)
μ	1.02 (0.09)	1.283	1.513	0.739	0.884	0.934 (0.102)
$\mu^{(1)}$	0.753 (0.012)	0.752	0.768		0.750	0.750 (0.011)
$\mu^{(2)}$	0.747 (0.009)	0.736	0.750		0.740	0.740 (0.009)

[a] Low-dipole configuration, from QUPID simulations at 20 K, see Ref. 24.
[b] Minimum energy configuration of the neutral water molecule.
[c] Minimum energy configuration of the neutral dimer.
[d] Equilibrium averaged configuration of the neutral dimer, at 20 K.

APPENDIX

In this Appendix we provide details of the geometries of the dimer configurations used in our studies of $(H_2O)_2^-$, along with structural parameters for the neutral dimer, $(H_2O)_2$, and the monomer. Values for various distances and angles characterizing the structures are given in Table VI, and are defined in Fig. 1. The values for the low-dipole (LD) configuration are obtained as average over the equilibrium ensemble generated via QUPID simulations,[24] at 20 K. The values for the ID and HD configurations are for typical single configurations selected from the QUPID simulations.[24] For the neutral monomer and dimer the minimum energy configuration is given, using the RWK2-M potentials.[39] For $(H_2O)_2$ equilibrium averaged values, at 20 K are also given. We note the substantial librational amplitude, at this temperature, of the acceptor molecule, indicated by the large standard deviation of the angle $\alpha^{(2)}$, both for the neutral and negatively charged LD configuration. In addition we observe the absence of significant differences in the intramolecular structure of the individual molecules between the neutral and the negatively charged dimer.

[1] M. Armbuster, H. Haberland, and H. G. Schindler, Phys. Rev. Lett. **47**, 323 (1981); H. Haberland, H. Langosch, H. G. Schindler, and D. R. Worsnop, Surf. Sci. **156**, 517 (1985).
[2] L. A. Posey and M. A. Johnson, J. Chem. Phys. **89**, 4807 (1988); L. A. Posey, M. J. Deluca, P. J. Campagnola, and M. A. Johnson, J. Phys. Chem. **93**, 1178 (1989).
[3] H. Haberland, H. G. Schindler, and D. R. Worsnop, Ber. Bunsenges. Phys. Chem. **88**, 270 (1984).
[4] H. Haberland, H. G. Schindler, and D. R. Worsnop, J. Chem. Phys. **81**, 3742 (1984).
[5] M. Knapp, O. Echt, D. Kreisle, and E. Recknagel, J. Chem. Phys. **85**, 636 (1986); J. Phys. Chem. **91**, 2601 (1987).
[6] (a) K. H. Bowen and J. G. Eaton, in *The Structure of Small Molecules and Ions*, edited by R. Naaman and Z. Vager (Plenum, New York, 1988), p. 147; (b) S. T. Arnold, J. G. Eaton, D. Patel-Misra, H. W. Sarkas, and K. H. Bowen, in *Ion Cluster Spectroscopy and Structure*, edited by J. P. Maier (Elsevier, Amsterdam, 1989).
[7] See articles, in *Elemental and Molecular Clusters*, edited by G. Benedek, T. P. Martin, and G. Pacchioni (Springer, Berlin, 1988).
[8] T. M. Miller, D. G. Leopold, K. K. Murray, and W. C. Lineberger, J. Chem. Phys. **85**, 2368 (1986), and references therein.
[9] T. P. Martin, Phys. Rep. **95**, 167 (1983), and references therein.
[10] (a) M. Kappes, P. Radi, M. Schar, and E. Schumacher, Chem. Phys. Lett. **113**, 243 (1985); (b) K. I. Peterson, P. D. Dao, and A. W. Castelman, Jr., J. Chem. Phys. **79**, 777 (1983); (c) E. C. Honea, M. L. Homer, P. Labastie, and R. L. Whethen, Phys. Rev. Lett. **63**, 394 (1989); (d) M. Kappes (to be published).
[11] (a) M. Newton, J. Chem. Phys. **58**, 5833 (1973); (b) B. K. Rao and N. R. Kestner, *ibid.* **80**, 1587 (1984).
[12] D. J. Chipman, J. Phys. Chem. **82**, 1980 (1978); **83**, 1657 (1979).
[13] K. H. Bennemann and P. Stampfli, Phys. Rev. Lett. **58**, 2635 (1987); P. Stanpfli and K. H. Bennemann, Phys. Rev. A **71**, 1674 (1988).
[14] K. D. Jordan, Acc. Chem. Res. **12**, 36 (1979).
[15] See Refs. 1–14 in Ref. 8.
[16] V. M. Nabutovskii and D. A. Romanov, Sov. J. Low Temp. Phys. **11**, 277 (1985); M. V. Rama Krishna and K. B. Whaley, Phys. Rev. B **38**, 11839 (1988).
[17] A. Wallqvist, D. Thirumalai, and B. J. Berne, J. Chem. Phys. **85**, 1583 (1986).
[18] See reviews by: (a) B. J. Berne and D. Thirumalai, Annu. Rev. Phys. Chem. **37**, 401 (1986); (b) M. Sprik and M. Klein, Comp. Phys. Rep. **7**, 147 (1988).
[19] See reviews by U. Landman, R. N. Barnett, C. L. Cleveland, J. Luo, D. Scharf, and J. Jortner, in *Few Body Systems and Multiparticle Dynamics*, edited by D. Micha (AIP, New York, 1987), p. 200; U. Landman, in *Recent Developments in Computer Simulation Studies in Condensed Matter Physics*, edited by D. P. Landau, K. K. Mon, and H. B. Schuttler (Springer, Berlin, 1988), p. 144.
[20] See review by J. Jortner, D. Scharf, and U. Landman, in Ref. 7, p. 148; R. N. Barnett, U. Landman, D. Scharf, and J. Jortner, Acct. Chem. Res. **22**, 350 (1989).
[21] D. Scharf, J. Jortner, and U. Landman, J. Chem. Phys. **88**, 4273 (1988).
[22] U. Landman, D. Scharf, and J. Jortner, Phys. Rev. Lett. **54**, 1860 (1985).
[23] R. N. Barnett, U. Landman, C. L. Cleveland, and J. Jortner, Phys. Rev. Lett. **59**, 811 (1987).
[24] U. Landman, R. N. Barnett, C. L. Cleveland, D. Scharf, and J. Jortner, J. Phys. Chem. **91**, 4890 (1987).
[25] R. N. Barnett, U. Landman, C. L. Cleveland, and J. Jortner, J. Chem. Phys. **88**, 4421 (1988).
[26] R. N. Barnett, U. Landman, C. L. Cleveland, and J. Jortner, J. Chem. Phys. **88**, 4429 (1988).
[27] R. N. Barnett, U. Landman, and J. Jortner, Chem. Phys. Lett. **145**, 382 (1988).

[28]R. N. Barnett, U. Landman, N. R. Kestner, and J. Jortner, J. Chem. Phys. **88**, 6670 (1988); Chem. Phys. Lett. **148**, 249 (1988).
[29]R. N. Barnett, U. Landman, and A. Nitzan, Phys. Rev. A **38**, 2178 (1988).
[30](a) R. N. Barnett, U. Landman, and A. Nitzan, J. Chem. Phys. **89**, 2242 (1988); (b) R. N. Barnett, U. Landman, and A. Nitzan (to be published).
[31]J. Jortner, U. Landman, and R. N. Barnett, Chem. Phys. Lett. **152**, 353 (1988).
[32](a) R. N. Barnett, U. Landman, and A. Nitzan, Phys. Rev. Lett. **62**, 106 (1989); see also J. Chem. Phys. **91**, 5567 (1989); (b) R. N. Barnett, U. Landman, G. Rajagopal, and A. Nitzan, Israel J. Chem. (to be published).
[33]R. N. Barnett, U. Landman, and A. Nitzan, J. Chem. Phys. **90**, 4413 (1989).
[34]M. Marchi, M. Sprik, and M. L. Klein, J. Chem. Phys. **89**, 4918 (1988).
[35]G. J. Martyna and B. J. Berne, J. Chem. Phys. **88**, 4516 (1988); **90**, 3744 (1989).
[36](a) M. D. Feit, J. A. Feit, Jr., and A. Steiger, J. Comput. Phys. **47**, 412 (1982); (b) M. D. Feit and J. A. Fleck, Jr., J. Chem. Phys. **78**, 301 (1983); **80**, 2578 (1984); (c) D. Kosloff and R. Kosloff, J. Comput. Phys. **52**, 35 (1983); (d) see review by R. Kosloff, J. Phys. Chem. **92**, 2087 (1988).
[37](a) P. A. M. Dirac, Proc. Cambridge Philos. Soc. **26**, 376 (1930); (b) D. Kumamoto and R. Silbey, J. Chem. Phys. **75**, 5164 (1981).
[38]See review by P. J. Rossky and J. Schnitker, J. Phys. Chem. **92**, 4277 (1988).
[39]For water we use the RWK2-M potential. See J. R. Reimers and R. O. Watts, Chem. Phys. **85**, 83 (1984); **64**, 95 (1982); see also Ref. 25.
[40]For the intermolecular interaction in ammonia we use the potential (model C) developed by A. Hinchliffe, D. G. Bounds, M. L. Klein, I. R. McDonald, and R. Righini, J. Chem. Phys. **74**, 1211 (1981), supplemented by intramolecular interactions modeled via a harmonic valence-coordinate model potential based on the one discussed by G. Herzberg in *Infrared and Raman Spectra* (Van Nostrand Reinhold, New York, 1945), Table 43, p. 177.
[41]The interatomic interactions which we employed in simulations of ionic clusters are discussed in D. Scharf, U. Landman, and J. Jortner, Chem. Phys. Lett. **130**, 5504 (1986); see also Refs. 19–22.
[42]J. Schnitker and P. J. Rossky, J. Chem. Phys. **86**, 3462, 3471 (1987).
[43]E. J. Hart and W. C. Gottschell, J. Am. Chem. Soc. **71**, 2101 (1969).
[44]R. P. Feynman and A. R. Hibbs, *Quantum Mechanics and Path Integrals* (McGraw–Hill, New York, 1965).
[45]D. Chandler and P. G. Wolynes, J. Chem. Phys. **79**, 4078 (1981); D. Chandler, J. Phys. Chem. **88**, 3400 (1984).
[46]M. F. Herman, E. J. Bruskin, and B. J. Berne, J. Chem. Phys. **76**, 5150 (1982).
[47]M. Parrinello and A. Rahman, J. Chem. Phys. **80**, 860 (1984).
[48]R. Kosloff and H. Talezer, Chem. Phys. Lett. **127**, 223 (1986).
[49]A. Selloni, P. Carenvali, R. Car, and M. Parrinello, Phys. Rev. Lett. **59**, 823 (1987), and Refs. 5–8 therein; see also D. Thirumalai, E. J. Bruskin, and B. J. Berne, J. Chem. Phys. **83**, 230 (1985).
[50]Z. Kotler, A. Nitzan, and R. Kosloff, in *Tunneling*, edited by J. Jortner and B. Pullman (Reidel, Boston, 1986), p. 193.
[51]Gaussian 86, M. J. Frisch, J. S. Binkley, H. B. Schlegel, K. Raghavachari, C. F. Melius, R. L. Martin, J. J. P. Stewart, F. W. Bobrowicz, C. M. Rohlfing, L. R. Kahn, D. J. Defrees, R. Seeger, R. A. Whiteside, D. J. Fox, E. M. Flueuder, and J. A. Pople, Carnegie-Mellon Quantum Chemistry Publishing Unit, Pittsburgh, PA, 1984.
[52]E. Clementi and Habitz, J. Phys. Chem. **87**, 2815 (1983).
[53]O. Matsuoka, E. Clementi, and M. Yoshimine, J. Chem. Phys. **64**, 1351 (1976).
[54]M. D. Newton and N. R. Kestner, Chem. Phys. Lett. **94**, 198 (1983).
[55]N. R. Kestner, M. D. Newton, and T. L. Mathers, Int. J. Quantum Chem. Symp. **17**, 431 (1983).
[56]C. H. Douglass, Jr., D. A. Weil, P. A. Charlier, R. A. Eades, D. G. Truhlar, and D. A. Dixon, *Chemical Applications of Atomic and Molecular Electrostatic Potentials*, edited by P. Politzer and D. G. Truhlar (Plenum, New York, 1981), p. 173.
[57]C. W. Kerr and M. Karplus, in *Water*, edited by F. Frank (Plenum, New York, 1972), p. 21.
[58]J. N. Bardsley, Case Stud. At. Phys. **4**, 299 (1974); G. G. Kleiman and U. Landman, Phys. Rev. B **8**, 5484 (1973).
[59]D. G. Truhlar, in Ref. 56, p. 123.
[60]C. Møller and M. S. Plesset, Phys. Rev. **46**, 618 (1934).
[61]T. R. Dyke, K. M. Mack, and J. S. Muenter, J. Chem. Phys. **66**, 498 (1977).